Meteoritics & Planetary Science 37, 1031–1043 (2002)
Available online at http://www.uark.edu/meteor

Boltysh, another end-Cretaceous impact

SIMON P. KELLEY[1]* AND EUGENE GUROV[2]

[1]Department of Earth Sciences, Open University, Walton Hall, Milton Keynes, MK7 6AA United Kingdom
[2]Institute of Geological Sciences, National Academy of Ukraine, 55-b Gontchar Str., Kiev, Ukraine
*Correspondence author's e-mail address: S.P.Kelley@open.ac.uk

(Received 2002 February 6; accepted in revised form 2002 April 29)

Abstract–The Chixculub impact occurred at the Cretaceous/Tertiary (K/T) boundary, and although several other Late Cretaceous and Paleogene impact craters have, at times, been linked with the K/T boundary, isotope geochronology has demonstrated that all have significantly different ages. The currently accepted age of the 24 km diameter Boltysh crater, a K-Ar whole-rock age, places it in the Coniacian at 88 ± 3 Ma. However, comprehensive Ar-Ar dating of a range of melt samples yields a mean age of 65.17 ± 0.64 Ma, within errors of the K/T boundary. Several of the fresh samples exhibit signs of excess argon but this seems to be concentrated in rapidly crystallized glass-rich samples.

The Ar-Ar age confirms an earlier fission track measurement and thus two dating techniques have yielded an age within errors of the K/T boundary for this crater. Crucially, although the ages of Boltysh and Chixculub are within errors, they may not have formed synchronously. Craters of 24 km diameter occur much more commonly than impacts of Chixculub dimensions, but their proximity does raise the important question of how many impacts there might have been close to the K/T boundary.

INTRODUCTION

Understanding the geology and environmental effects of terrestrial impacts has been the focus of much work since Alvarez *et al.* (1980) demonstrated the importance of an extraterrestrial influence upon the end-Cretaceous mass extinction. The search for a suitable crater saw several terrestrial craters fall under suspicion. The Manson crater in the USA was one of the original candidates, although at only 35 km it was too small to have caused the mass extinction (Kunk *et al.*, 1989). More recently however, Izett *et al.* (1993) measured an age of 73.8 Ma for a sanidine clast from Manson crater and Zeitler (1996) measured an age of 73.3 ± 0.2 Ma on shocked K-feldspars. Kara and Ust-Kara craters in Russia were also thought to be coincident with the K/T boundary on the basis of K-Ar analysis of glassy rocks from the ejecta layer which yielded an age of 66 ± 0.8 Ma (Shukulokov *et al.*, 1988). However these twin craters were also shown to have older ages; Ust-Kara yielded ages in the range 71–81 Ma (Koeberl *et al.*, 1990) and Kara has yielded an age of 70.3 ± 2.2 Ma (Trieloff *et al.*, 1998). Several other craters have also been linked with the K/T boundary but with little evidence. The Chixculub crater has remained the only crater to be confirmed with an isotopic age within errors of the accepted K/T boundary.

A great deal of interest centered upon the idea of multiple simultaneous impacts after the original work of Alvarez *et al.* (1980), but the discovery of the Chixculub crater, and particularly the fact that it was large enough to explain almost all the phenomena seen at the K/T boundary (Smit, 1999), has encouraged the image of a single massive impact. However, the concept of impact clusters has found favor in galactic theories to explain possible periodicity in cratering and synchronicity of the periods with mass extinctions (Rampino, 1998). The most notable coincidence of craters is that of Chesapeake Bay with a probable age of 35.4 ± 0.6 Ma (Glass *et al.*, 1986) and the Popigai crater dated at 35.7 ± 0.2 Ma (Bottomley *et al.*, 1997) though they were probably not synchronous impacts. These craters also fell during a time of heightened comet activity indicated by elevated levels of ^{3}He in oceanic sediments (Farley *et al.*, 1998). However sediments across the K/T boundary did not exhibit elevated levels of ^{3}He (Farley *et al.*, 1998). Impact clusters have also been described around the Frasnian–Famennian boundary at 364 Ma (Claeys and Casier, 1994) in the mid-Norian ~214 Ma (Spray *et al.*, 1998) and at the end of the Jurassic period ~144 Ma (Koeberl *et al.*, 1997).

The Boltysh crater (Fig. 1) is a complex impact structure, 24 km in diameter, situated in the central part of the Ukrainian Shield, centered at 48°45' N and 32°10' E in the basin of the Tyasmin river, a tributary of the Dnieper river (Fig. 1a). The crater is surrounded by an ejecta blanket represented by a multimict breccia layer preserved over an area of ~6500 km^2

Prelude preprint MS#4758

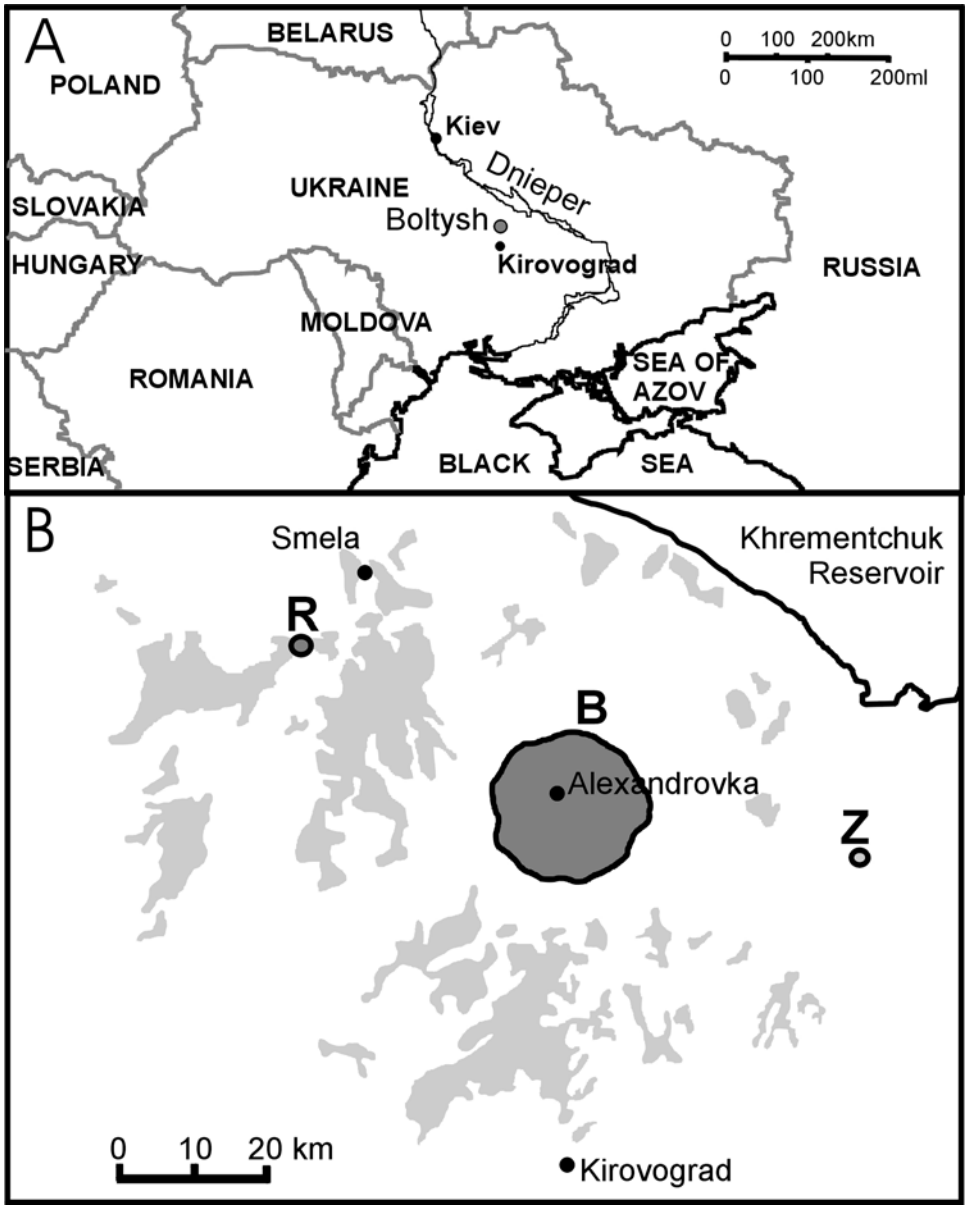

FIG. 1. (a) The Boltysh Impact crater lies in central Ukraine, north of Kirovograd. (b) The ejecta (pale shade) are distributed around the buried Boltysh impact crater (dark shade, marked "B"). Two other craters lie within this area, the Rotmistrakovka (marked "R") and Zeleny Gay (marked "Z") craters.

(Fig. 1b), but the fall-back or suevite ejecta is preserved only within the crater overlying an impact-melt sheet. The initial thickness of Boltysh ejecta was probably ~600 m at the crater rim, dropping to ~10 m at a distance of 47 km (3.9 crater radii) and further to ~1 m at the distance ~90 km from the center of the structure (Gurov *et al.*, 2001), covering an initial area of greater than ~25 000 km^2 to this depth. Although this area of ejecta coverage might be devastating to a densely populated nation hit by such an impact today, it is small in comparison with the worldwide distribution of ejecta of the Chixculub impact.

PREVIOUS CONSTRAINTS ON THE AGE OF THE BOLTYSH IMPACT

The age of the Boltysh crater and its ejecta have been approximately constrained using the local stratigraphy (Gurov and Gurova, 1991), but the constraints are limited because the crater is located in the axial part of the Ukrainian Shield which has not experienced a marine transgression since the early Paleozoic era. The northeastern slopes of the shield, including the area of the Tyasmin river basin, were however covered during a short period of the Cenomanian–Turonian

transgression. Cenomanian and Turonian sediments are preserved within the 3 km diameter Rotmistrovka impact structure, 45 km northwest of the Boltysh impact (Fig. 1a) (Gurov *et al.*, 2001), where they are overlain by an ejecta layer up to 18 m thick from the Boltysh impact event (Gurov and Babina, 2000; Gurov and Gurova, 1991). Thus, the lower limit of age of the Boltysh structure and its ejecta is Cenomanian–Turonian.

The upper age limit of the Boltysh ejecta is constrained by the age of Tertiary sediments overlying impact deposits within the crater. Although the upper contact of the impact sediments with the overlying deposits is not exposed, it has been traced in numerous bore holes within the crater (Gurov *et al.*, 2001). The oldest series, which lie on the surface of the impact-melt sheet and fall-back suevites, are silts and sands with thin interlayers of sedimentary breccia apparently free of flora and fauna. The lower series are overlain by ~300 m of shales, argillites and oil shales with abundant ostracoda, gastropoda, fishes and many flora. Investigations of the macrofossils by Stanislavsky (1968) using samples from core 1715, determined a probable Thanetian age for the lowermost series. Thus the age of the Boltysh crater and its ejecta are stratigraphically constrained to lie between Cenomanian–Turonian and Late Paleocene.

Until the present study, radiometric dating of Boltysh impact-melt rocks was limited to determinations by the K-Ar and fission track methods. The earliest investigations of two samples of glassy impact-melt rocks by the fission track method determined ages of 96 ± 10 Ma and 105 ± 13 Ma (Komarov and Raichlin, 1976) though the data were not fully presented. However, more recent dating of a core sample has been undertaken by Kashkarov *et al.* (1998), who performed a detailed analysis of impact-melt rock with plagioclase and hypersthene microcrystals from drill hole 11475 at a depth of 762 m. Kashkarov *et al.* (1998) corrected the age for annealing of fossil tracks and all samples were analysed for their chemical composition. The sample yielded an age of 65.0 ± 1.1 Ma (1σ errors) (Kashkarov *et al.*, 1998). While the age is within errors of the end-Cretaceous, the true age may be several million years from the Chixculub event.

Numerous K-Ar age determinations of glassy impact melts from the Boltysh crater have yielded a wide range of apparent ages. The most recent K-Ar date for the Boltysh crater was 88 ± 3 Ma (Boiko *et al.*, 1985), which has been the age most often quoted for the Boltysh impact (*e.g.*, Grieve, 1991). However, an age of 88 Ma is difficult to reconcile with geology of the Boltysh crater. The cavity formed by the impact was filled by a freshwater lake, abundant evidence for which is preserved in the oil shales, but if the impact occurred at 88 Ma, there must have been a gap of roughly 28 Ma before the Paleogene oil shales accumulated in the lake. Perhaps a more likely scenario would be that the lake became established in the cavity soon after the impact. Although initial deposits might reflect a poisonous lake environment while water was heated by the hydrothermal action in the crater, this stage would not be expected to last 28 Ma.

COMPOSITION AND PETROGRAPHY OF THE IMPACT MELT SHEET

The composition and petrography of the melt sheet within the two cores of the Boltysh crater were reported in detail by Grieve *et al.* (1987), who noted its particularly high silica contents (71 to 73 wt%) in comparison with other melt sheets. Grieve *et al.* (1987) concluded that the melt had originally been glassy throughout but that some levels had had evolved to devitrified glass and microcrystalline rock. Around 60 m at the top of the melt sheet is completely microcrystalline and although bore hole B50 did not penetrate basement, the lowest portions in another bore hole B11475 are also microcrystalline (Grieve *et al.*, 1987). The central zones are fresh glasses or partially devitrified glass, in contrast to some other melt sheets which are more crystalline in their core (Grieve *et al.*, 1987). Grieve *et al.* (1987) attributed this feature to the high silica content of the melt, together with relatively high alumina and alkali contents which made the melt extremely viscous and also inhibited crystal nucleation. Devitrification and crystal nucleation were highest where crustal fluids were in close contact with the melt at the lower and particularly the upper boundary.

Glass-rich zones contain ~20% plagioclase phenocrysts (An_{40-55}) up to 100 μm in length in the samples we have studied (Grieve *et al.* report phenocrysts up to 1 mm), exhibiting "hopper" or "swallow tail" morphologies (Fig. 2a,b), indicating rapid growth. In addition, glassy and partially devitrified rocks also contain ~10% pyroxene phenocrysts. Microcrystalline melt rocks contain up to 25% feldspar phenocrysts with plagioclase cores of similar composition to the glassy samples but they also exhibit sanidine rims (Fig. 2c,d). In addition the microcrystalline rocks also contain some (up to 5%) biotite and chlorite pseudomorphing pyroxene (Grieve *et al.*, 1987). Samples from all these horizons have been analysed. Granite clasts are present in all samples though they are assimilated to varying extents.

SAMPLE CHARACTERIZATION AND ARGON-ARGON DATING

Seven samples of impact melt were selected from drill cores recovered from a variety of depths in drill hole number 50 in the Boltysh Crater, which penetrated the impact-melt horizon surrounding the central uplift (Grieve *et al.*, 1987). The melt is contaminated by clasts of quartz and feldspar and contains feldspar phenocrysts generally <100 μm in length. In many samples even though the plagioclase grains may be up to 100 μm in length, the "hopper" shapes of the plagioclase phenocrysts with large melt inclusions (Fig. 2) make mineral separation difficult. Samples were prepared initially as thick sections for

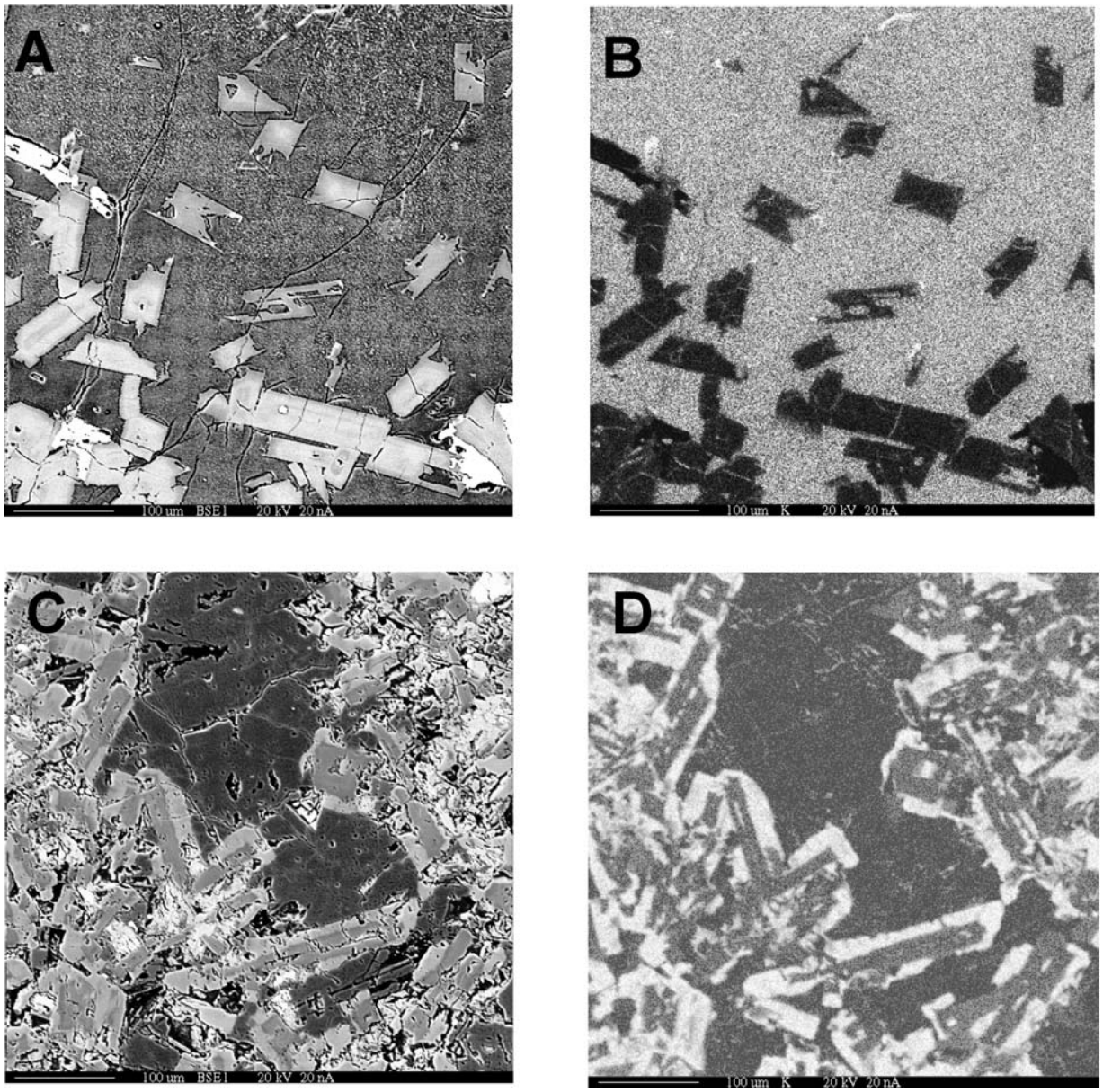

FIG. 2. (a) SEM backscatter "Z-contrast" image of impact melt, sample 50/622, showing "hopper" style plagioclase crystals in cracked glass. (b) X-ray map of potassium distribution in the same view of sample 50/622. Note that the lighter shade in the glass indicates that potassium is concentrated in this phase. (c) SEM backscatter "Z-contrast" image of impact melt, sample 50/736. In this sample, plagioclase crystals show growth zoning. (d) X-ray map of potassium distribution in sample 50/736. In contrast to sample 50/622, the lighter shades show that potassium is concentrated in the feldspar crystals, particularly in the crystal rims.

laser spot dating, but subsequently 1 mm diameter clast-poor fragments of melt were picked for laser stepped heating. Both the glass content and composition of samples varies greatly and this has a marked effect upon the release of argon from the samples and upon the recovery of meaningful ages from the samples.

Samples of impact melt were wrapped in aluminium foil and irradiated at the McMaster reactor, Canada and the GA1550 biotite standard, with an age of 98.79 ± 0.96 Ma (Renne *et al.*, 1998), was used to monitor the fast-neutron flux. For the laser spot experiments, spots on polished rock slices were melted using short (~10 ms) laser pulses using a focused CW Nd-YAG infrared laser with an external shutter; individual fragments of impact melt were heated using the same laser. The released gases were cleaned by Zr-Al getters and argon isotopes were measured in a MAP 215-50 noble gas mass spectrometer. Analyses were corrected for blanks, ^{37}Ar decay and neutron-induced interference reactions. All errors on spot ages, total gas ages and plateau ages are quoted at the 2σ level.

An initial experiment was undertaken using laser spot analysis on samples from 658.5 to 729.5 m which appeared to exhibit very little alteration and were relatively clast free. Ages from sample 658.5 ranged from 91.69 ± 1.95 to 100.71 ± 1.93 Ma (Table 1; Fig. 3a) with a mean of 95.9 ± 3.4 Ma, whereas samples 729.5 yielded ages in the range 70.87 ± 4.56 and 78.81 ± 3.7 Ma (Table 1; Fig. 3a) with a mean of 75.1 ± 0.7 Ma. The unusually large errors of the second sample are a result of small sample sizes used in order to avoid clasts which it was thought might cause interference. However, where clasts were encountered, their presence did not significantly affect the ages. Several observations can be made on the basis of this data; the ages were clustered for each sample but not reproducible between samples, and variations were unrelated to atmospheric contamination or the abundance of basement mineral clasts. These two samples were selected from the freshest glass-rich zones (Fig. 4) and these observations lead us to believe that the spread in ages result from excess argon, probably dissolved in the glass, rather than argon in clasts or excess argon introduced by hydrothermal activity and later alteration. Further, the excess argon in the glass may be better described as inherited argon since it probably originated as radiogenic argon in the target rock, which did not escape during the impact and quench. The data on Fig. 3a appear to show near horizontal trends with very low abundances of atmospheric argon, and they can not be used to identify the isotope ratio of an excess component other than pure ^{40}Ar. Moreover, the younger sample yielded an age considerably younger than the previously accepted K-Ar age for Boltysh of 88 ± 3 Ma. Subsequent samples selected for analysis were crystal-rich rocks which may have had longer cooling histories, and a laser step-heating technique was used to achieve better precision, since clasts did not appear to be the source of older ages and thus were not likely to contain significant inherited argon.

Subsequent analysis of five samples yielded younger and more reproducible ages and electron microprobe analyses helped to explain some of the age variations which remained. The deepest sample, from 736 m, yielded a very scattered release spectrum (Fig. 3b) with ages ranging from 88.94 ± 0.77 to 97.09 ± 0.54 Ma (Table 2), very similar to the sample from 658.5 m. There was no strong correlation between age and Cl/K, Ca/K or atmospheric content. Electron microprobe analysis however indicated a possible reason for the retention of excess argon in this sample. Figure 2a shows a scanning

TABLE 1. Laser spot melted samples.

Sample	Material melted	$^{40}Ar/^{39}Ar$	$^{38}Ar/^{39}Ar$	$^{37}Ar/^{39}Ar$	$^{36}Ar/^{39}Ar$	$^{40}Ar^*/^{39}Ar$	%Atm	Age* (Ma)
50/658.5	*J* value = 0.005406							
Spot 1	Matrix	10.473	0.0283	0.000	0.00059	10.299	98.3	97.66 ± 0.93
Spot 2	Matrix	10.049	0.0278	0.002	0.00129	9.668	96.2	91.82 ± 1.61
Spot 3	Matrix	10.873	0.0291	0.000	0.00082	10.630	97.8	100.71 ± 1.93
Spot 4	Matrix	10.228	0.0278	0.001	0.00112	9.896	96.8	93.94 ± 2.20
Spot 5	Matrix	10.170	0.0262	0.004	0.00134	9.773	96.1	92.80 ± 2.11
Spot 6	Matrix	10.702	0.0312	0.000	0.00052	10.548	98.6	99.96 ± 1.79
Spot 7	Matrix	10.057	0.0266	0.004	0.00136	9.654	96.0	91.70 ± 1.66
Spot 8	Matrix	10.379	0.0282	0.001	0.00089	10.114	97.5	95.96 ± 1.67
Spot 9	Matrix	10.759	0.0280	0.000	0.00070	10.553	98.1	100.00 ± 1.23
Spot 10	Matrix	10.560	0.0288	0.001	0.00057	10.392	98.4	98.52 ± 1.79
Spot 11	Matrix	9.832	0.0294	0.001	0.00061	9.653	98.2	91.69 ± 1.95
Weighted mean								95.89 ± 3.46
50/729.5	*J* value = 0.005401							
Spot 1	Matrix	7.842	0.0148	0.002	0.00000	7.842	100.0	74.84 ± 2.63
Spot 2	Matrix and clast	7.871	0.0131	0.000	0.00021	7.809	99.2	74.53 ± 4.81
Spot 3	Clast	7.773	0.0134	0.002	0.00000	7.773	100.0	74.19 ± 4.16
Spot 4	Clast	7.779	0.0148	0.000	0.00122	7.418	95.4	70.87 ± 4.56
Spot 5	Matrix	7.720	0.0094	0.003	0.00000	7.720	100.0	73.70 ± 5.49
Spot 6	Matrix	8.024	0.0159	0.003	0.00000	8.024	100.0	76.54 ± 3.61
Spot 7	Matrix and clast	8.268	0.0129	0.000	0.00000	8.268	100.0	78.81 ± 3.70
Spot 8	Matrix and clast	7.929	0.0205	0.000	0.00020	7.871	99.3	75.11 ± 4.67
Spot 9	Matrix	7.497	0.0234	0.005	0.00000	7.497	100.0	71.61 ± 11.14
Weighted mean								75.08 ± 0.73

All analytical errors shown at 2σ with *J* value errors included.
*All final age errors at 95% confidence level.

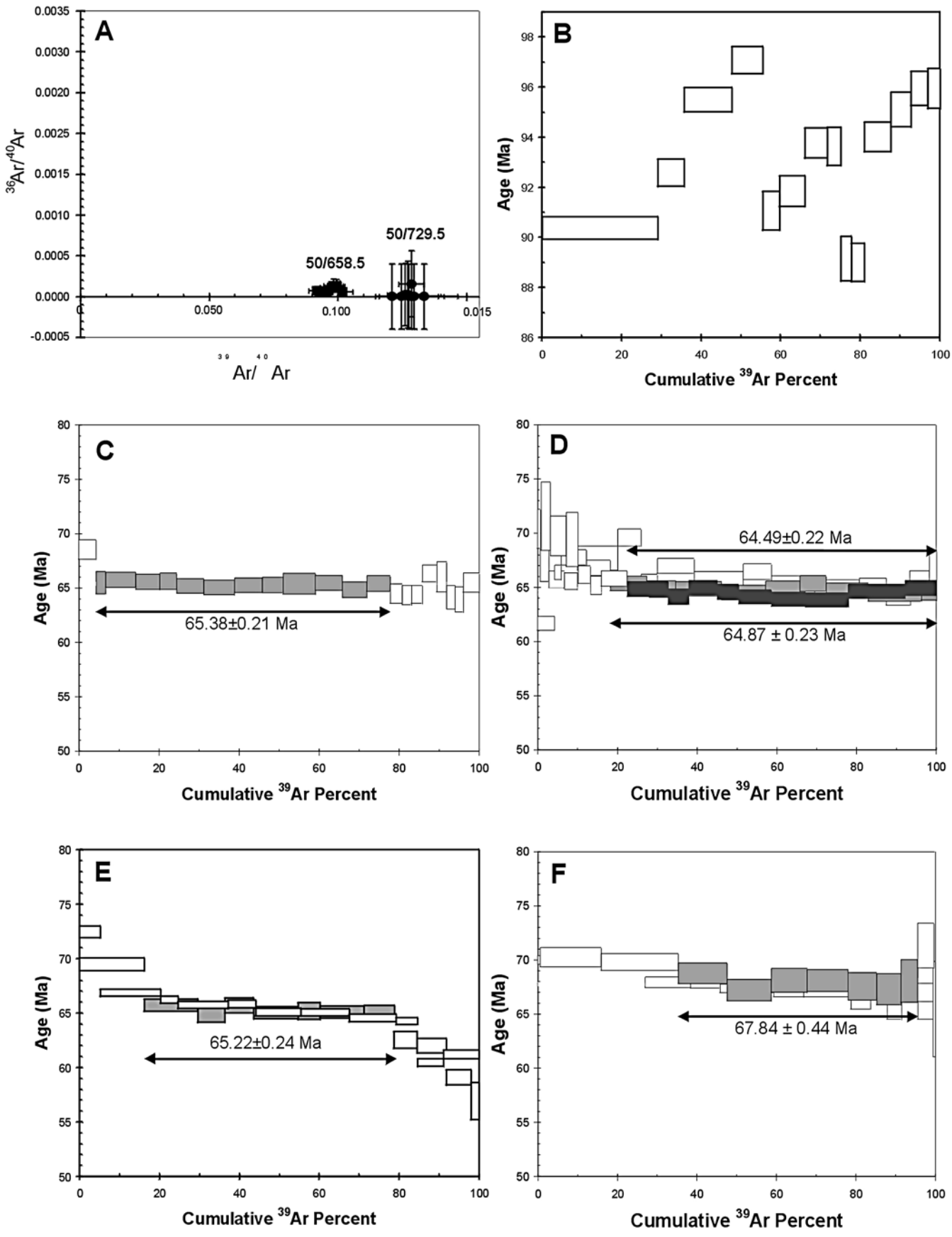
A
$^{36}Ar/^{40}Ar$
$^{39}Ar/^{40}Ar$
50/729.5
50/658.5
B
Age (Ma)
Cumulative ^{39}Ar Percent
C
Age (Ma)
65.38±0.21 Ma
Cumulative ^{39}Ar Percent
D
Age (Ma)
64.49±0.22 Ma
64.87 ± 0.23 Ma
Cumulative ^{39}Ar Percent
E
Age (Ma)
65.22±0.24 Ma
Cumulative ^{39}Ar Percent
F
Age (Ma)
67.84 ± 0.44 Ma
Cumulative ^{39}Ar Percent

FIG. 3. (*left*) Ar-Ar correlation diagram of the first two samples analysed using a spot technique, and release spectra of the remaining samples analysed by stepwise Ar release. All boxes in the release spectra are shown at the 2σ level. (a) Plot of spot data from samples 50/658.5 and 50/729.5, showing near horizontal spreads towards the origin, no isochron could be defined. (b) Stepped-heating release from one aliquot of sample 50/736. (c) Stepped-heating release from one aliquot of sample 50/710, showing a plateau age of 65.38 ± 0.21 Ma. (d) Stepped-heating release from three aliquots of sample 50/652, two of which defined plateaus at 64.49 ± 0.22 and 64.87 ± 0.23 Ma. (e) Stepped-heating release from two aliquots of sample 50/622, one of which defined a plateau age of 65.4 ± 0.24 Ma. (f) Stepped-heating release from two aliquots of sample 50/605, one of which defined a plateau age of 67.84 ± 0.44 Ma.

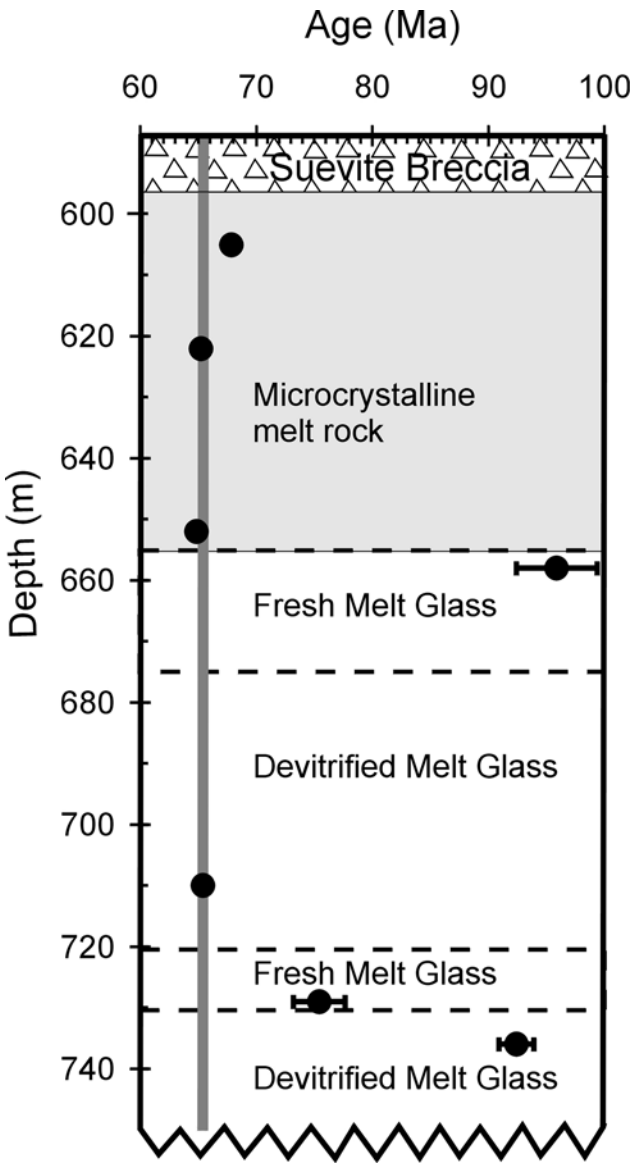

FIG. 4. Age *vs.* depth profile for samples dated from Boltysh bore hole 50 from Grieve *et al.* (1987) with additional ages from the present study. The lower melt zones in this bore hole exhibit fresh and partially devitrified glass and are overlain by a zone in which the melt became more crystalline (shown in grey shade). The melt is overlain by a suevite breccia. The mean or plateau sample ages are shown as closed circles. The K/T boundary is shown at 65.4 Ma, as a vertical grey line.

electron microscope (SEM) Z-contrast image of sample 50/736 showing simple crystals of plagioclase and clinopyroxene in a homogeneous glass. Although this sample was derived from a zone dominated by devitrified glass (Fig. 4) (Grieve *et al.*, 1987), sample 50/736 contained relatively fresh glass. Figure 2b shows that potassium is concentrated in the glass, demonstrating that the Ar-Ar release spectrum was dominated by argon release from glass. Electron microprobe analyses indicate a mean of 4.5% K_2O in the glass and 0.47% in plagioclase. Moreover cracks in the plagioclase crystals also contain potassium, probably in the form of clay minerals. The lack of zoning, and small hopper-shaped crystals containing melt inclusions indicate formation and crystallization in a rapidly cooling melt. Perhaps like the samples analysed in the earlier experiment, this sample formed and froze before radiogenic argon inherited from the precursor target rocks of pre-Cambrian basement could completely outgas.

The next highest sample, at 710 m (Table 2; Fig. 3c) was more crystal rich but also indicated a more complex crystallization history. Most areas of melt yielded K_2O contents with a mean of 3.1% K_2O, but one area, possibly a clast of an earlier melt, contained many clinopyroxene crystals and a mean of 5.1% K_2O. Plagioclase crystals were unzoned, containing a mean of 0.46% K_2O and clinopyroxene contained little potassium. Stepped-heating analysis of sample 50/710 revealed a plateau over 73.5% of ^{39}Ar release with an mean age of 65.38 ± 0.21 Ma (2σ errors, calculated using ISOPLOT/Ex; Ludwig, 1999) (Fig. 3c). The plateau age is dominated by argon released from glass since it contains an order of magnitude more potassium than any other phase; the slightly variable ages in the final 20% of ^{39}Ar release may result from the combination of feldspar clasts and plagioclase crystals in the melt. The Ca/K ratio is initially high, in the region of 0.4, but falls to 0.24 before rising in the last 20% ^{39}Ar release to 0.28, probably reflecting the contributions from clasts and plagioclase.

The next highest sample, 50/652 is very different, containing zoned feldspars and glass with low potassium contents. The glass is also variably devitrified and microcrystalline. This rock evolved further before freezing and exhibits feldspar laths with plagioclase cores and alkali rims. Feldspar cores typically contain 0.48% K_2O and rims, which make up over half the crystal volumes, contain up to 10.3% K_2O. Three experiments were undertaken on different aliquots of this sample. The first experiment did not yield a plateau (Fig. 3d), although step ages varied only between 64.13 ± 0.76 and 70.45 ± 1.81 Ma (Table 2) and yielded a mean age of 66.06 ± 0.74. A second aliquot was analysed, taking care to gently heat the sample thoroughly in

TABLE 2. Laser step heated samples.

	$^{40}Ar/^{39}Ar$	$^{38}Ar/^{39}Ar$	$^{37}Ar/^{39}Ar$	$^{36}Ar/^{39}Ar$	%Atm	$^{40}Ar^*/^{39}Ar$	$\%^{39}Ar$	Age* (Ma)
50/536	*J* value† = 0.009817							
Step 1	5.843	0.0132	0.157	0.00208	89.5	5.230	28.86	90.32 ± 0.46
Step 2	5.881	0.0130	0.184	0.00175	91.2	5.362	35.70	92.55 ± 0.55
Step 3	5.919	0.0117	0.316	0.00129	93.6	5.538	47.52	95.50 ± 0.49
Step 4	5.953	0.0122	0.378	0.00109	94.6	5.632	55.38	97.09 ± 0.54
Step 5	5.765	0.0121	0.417	0.00167	91.4	5.271	59.67	91.02 ± 0.77
Step 6	5.744	0.0113	0.488	0.00144	92.6	5.318	65.97	91.82 ± 0.61
Step 7	5.786	0.0120	0.473	0.00119	93.9	5.434	71.50	93.76 ± 0.60
Step 8	5.742	0.0126	0.516	0.00107	94.5	5.425	74.89	93.60 ± 0.77
Step 9	5.685	0.0128	0.608	0.00179	90.7	5.157	77.67	89.09 ± 0.89
Step 10	5.836	0.0127	0.566	0.00233	88.2	5.148	80.98	88.94 ± 0.77
Step 11	5.808	0.0111	0.460	0.00122	93.8	5.448	87.53	94.00 ± 0.60
Step 12	5.876	0.0116	0.449	0.00123	93.8	5.513	92.65	95.09 ± 0.70
Step 13	5.888	0.0118	0.417	0.00110	94.5	5.564	96.81	95.94 ± 0.69
Step 14	5.963	0.0127	0.876	0.00135	93.3	5.565	100.00	95.96 ± 0.81
Weighted mean								93.30 ± 1.50
50/605 (A)	*J* value = 0.00645							
Step 1	6.907	0.0141	0.220	0.00260	88.9	6.138	26.99	70.04 ± 0.39
Step 2	6.069	0.0140	0.158	0.00040	98.1	5.952	38.46	67.96 ± 0.49
Step 3	6.009	0.0146	0.134	0.00020	99.0	5.951	45.79	67.95 ± 0.51
Step 4	6.067	0.0146	0.136	0.00056	97.3	5.902	59.34	67.41 ± 0.39
Step 5	6.010	0.0145	0.109	0.00045	97.8	5.877	66.94	67.13 ± 0.50
Step 6	6.034	0.0150	0.114	0.00055	97.3	5.870	78.82	67.05 ± 0.41
Step 7	6.146	0.0143	0.118	0.00122	94.1	5.787	83.72	66.11 ± 0.63
Step 8	6.320	0.0135	0.159	0.00125	94.1	5.950	87.80	67.94 ± 0.76
Step 9	6.291	0.0144	0.232	0.00194	90.9	5.719	91.55	65.35 ± 0.81
Step 10	6.366	0.0131	0.244	0.00103	95.2	6.063	95.64	69.21 ± 0.77
Step 11	6.272	0.0144	0.235	0.00187	91.2	5.718	99.36	65.35 ± 0.82
Step 12	6.245	0.0175	0.245	0.00174	91.8	5.732	100.00	65.50 ± 4.41
Weighted mean								67.73 ± 0.87
50/605 (B)								
Step 1	6.765	0.0151	0.238	0.00208	90.9	6.150	15.42	70.18 ± 0.88
Step 2	6.194	0.0129	0.177	0.00028	98.7	6.110	35.02	69.74 ± 0.80
Step 3	6.087	0.0138	0.172	0.00024	98.8	6.016	47.37	68.68 ± 0.97
Step 4	6.044	0.0156	0.163	0.00057	97.2	5.877	58.59	67.12 ± 0.99
Step 5	6.062	0.0148	0.126	0.00035	98.3	5.958	67.70	68.03 ± 1.11
Step 6	6.120	0.0153	0.130	0.00056	97.3	5.955	78.00	68.00 ± 1.03
Step 7	6.118	0.0137	0.113	0.00071	96.6	5.908	85.24	67.47 ± 1.29
Step 8	6.255	0.0136	0.135	0.00125	94.1	5.886	91.43	67.23 ± 1.46
Step 9	6.537	0.0134	0.237	0.00197	91.1	5.953	95.70	67.98 ± 2.00
Step 10	6.615	0.0124	0.243	0.00124	94.4	6.247	99.79	71.27 ± 2.10
Step 11	12.748	0.0054	0.144	0.02215	48.7	6.202	100.00	70.77 ± 38.39
Weighted mean								68.88 ± 0.83
Plateau								67.84 ± 0.44
50/622 (A)	*J* value = 0.006451							
Step 1	12.584	0.0186	0.196	0.02109	50.5	6.352	5.26	72.45 ± 0.52
Step 2	6.284	0.0138	0.218	0.00146	93.1	5.852	20.28	66.85 ± 0.33
Step 3	6.007	0.0134	0.178	0.00072	96.5	5.795	24.66	66.21 ± 0.35
Step 4	5.968	0.0156	0.181	0.00073	96.4	5.752	37.19	65.74 ± 0.33
Step 5	5.847	0.0148	0.155	0.00030	98.5	5.759	44.13	65.81 ± 0.34
Step 6	5.922	0.0185	0.147	0.00077	96.1	5.694	55.45	65.08 ± 0.33
Step 7	5.835	0.0191	0.103	0.00049	97.5	5.691	67.66	65.05 ± 0.32

TABLE 2. *Continued.*

	$^{40}Ar/^{39}Ar$	$^{38}Ar/^{39}Ar$	$^{37}Ar/^{39}Ar$	$^{36}Ar/^{39}Ar$	%Atm	$^{40}Ar^*/^{39}Ar$	$\%^{39}Ar$	Age* (Ma)
50/622 (A) *Continued*								
Step 8	5.763	0.0197	0.088	0.00039	98.0	5.647	79.28	64.55 ± 0.35
Step 9	5.716	0.0200	0.090	0.00033	98.3	5.618	84.63	64.22 ± 0.34
Step 10	5.516	0.0194	0.124	0.00080	95.7	5.279	91.08	60.42 ± 0.33
Step 11	5.701	0.0187	0.126	0.00120	93.8	5.347	100.00	61.18 ± 0.39
Weighted mean								64.60 ± 1.50
50/622 (B)								
Step 1	8.292	0.0163	0.240	0.00747	73.4	6.085	16.28	69.46 ± 0.59
Step 2	5.988	0.0151	0.198	0.00080	96.1	5.752	29.62	65.72 ± 0.56
Step 3	5.859	0.0159	0.146	0.00064	96.8	5.670	36.33	64.80 ± 0.69
Step 4	5.933	0.0164	0.134	0.00062	96.9	5.749	43.51	65.68 ± 0.67
Step 5	5.925	0.0211	0.119	0.00080	96.0	5.689	54.78	65.01 ± 0.57
Step 6	5.851	0.0209	0.100	0.00051	97.4	5.701	60.29	65.14 ± 0.77
Step 7	5.830	0.0229	0.086	0.00046	97.7	5.694	71.36	65.07 ± 0.57
Step 8	5.831	0.0194	0.079	0.00048	97.6	5.689	78.80	65.01 ± 0.66
Step 9	5.805	0.0190	0.119	0.00115	94.2	5.466	84.52	62.51 ± 0.75
Step 10	5.827	0.0167	0.124	0.00138	93.0	5.419	91.84	61.98 ± 0.65
Step 11	5.950	0.0181	0.122	0.00268	86.7	5.158	98.01	59.04 ± 0.70
Step 12	6.080	0.0194	0.113	0.00377	81.7	4.966	100.00	56.88 ± 1.73
Weighted mean								64.60 ± 1.70
Plateau								65.22 ± 0.24
50/652 (A)	*J* value = 0.009809							
Step 1	19.643	0.0225	0.183	0.05274	20.7	4.060	0.73	70.45 ± 1.81
Step 2	15.508	0.0207	0.191	0.03941	24.9	3.863	2.86	67.09 ± 1.51
Step 3	4.936	0.0133	0.195	0.00390	76.7	3.784	6.75	65.76 ± 0.77
Step 4	4.625	0.0133	0.193	0.00288	81.6	3.775	10.04	65.59 ± 0.76
Step 5	5.221	0.0129	0.201	0.00447	74.7	3.900	20.10	67.73 ± 1.11
Step 6	6.133	0.0133	0.183	0.00718	65.4	4.013	25.99	69.65 ± 0.80
Step 7	4.192	0.0117	0.181	0.00143	89.9	3.769	30.01	65.49 ± 0.76
Step 8	4.722	0.0128	0.202	0.00293	81.7	3.857	39.25	67.00 ± 0.69
Step 9	4.452	0.0125	0.196	0.00225	85.1	3.788	51.55	65.82 ± 0.69
Step 10	5.276	0.0127	0.178	0.00491	72.5	3.826	58.61	66.47 ± 0.71
Step 11	4.694	0.0133	0.179	0.00315	80.2	3.763	69.42	65.39 ± 0.69
Step 12	4.739	0.0132	0.168	0.00337	79.0	3.742	80.65	65.04 ± 0.70
Step 13	4.191	0.0125	0.154	0.00150	89.4	3.748	87.42	65.14 ± 0.73
Step 14	4.212	0.0132	0.161	0.00177	87.6	3.689	93.36	64.13 ± 0.76
Step 15	4.397	0.0130	0.160	0.00208	86.0	3.783	98.16	65.72 ± 0.83
Step 16	4.507	0.0134	0.143	0.00220	85.6	3.858	100.00	67.01 ± 1.41
Weighted mean								66.06 ± 0.74
50/652 (B)								
Laser step 1	202.010	0.1172	0.619	0.59008	13.7	27.640	0.17	432.80 ± 74.28
Laser step 2	48.151	0.0369	0.222	0.12910	20.8	10.003	0.50	168.86 ± 10.05
Laser step 3	18.287	0.0246	0.211	0.04663	24.7	4.509	0.92	78.08 ± 8.44
Laser step 4	9.896	0.0156	0.232	0.01952	41.7	4.128	3.23	71.60 ± 3.16
Laser step 5	5.521	0.0124	0.228	0.00507	72.8	4.021	7.28	69.80 ± 1.84
Laser step 6	4.599	0.0113	0.250	0.00202	87.0	4.001	10.14	69.45 ± 2.50
Laser step 7	4.463	0.0125	0.247	0.00221	85.4	3.810	13.26	66.20 ± 0.82
Laser step 8	4.406	0.0128	0.282	0.00221	85.2	3.753	16.02	65.23 ± 0.84
Laser step 9	4.279	0.0120	0.272	0.00165	88.6	3.790	22.47	65.86 ± 0.72
Laser step 10	4.117	0.0126	0.258	0.00130	90.7	3.733	28.03	64.88 ± 0.70
Laser step 11	4.127	0.0125	0.240	0.00135	90.4	3.730	32.75	64.82 ± 0.76
Laser step 12	4.169	0.0127	0.239	0.00161	88.6	3.692	37.90	64.17 ± 0.73

TABLE 2. *Continued.*

	$^{40}Ar/^{39}Ar$	$^{38}Ar/^{39}Ar$	$^{37}Ar/^{39}Ar$	$^{36}Ar/^{39}Ar$	%Atm	$^{40}Ar^*/^{39}Ar$	$\%^{39}Ar$	Age* (Ma)
50/652 (B) *Continued*								
Laser step 13	4.155	0.0124	0.216	0.00140	90.0	3.740	44.99	65.00 ± 0.67
Laser step 14	4.196	0.0128	0.171	0.00162	88.6	3.717	50.42	64.61 ± 0.70
Laser step 15	4.207	0.0126	0.144	0.00175	87.7	3.689	58.68	64.14 ± 0.66
Laser step 16	4.234	0.0122	0.104	0.00188	86.9	3.678	67.19	63.93 ± 0.65
Laser step 17	4.300	0.0126	0.089	0.00212	85.5	3.674	77.89	63.88 ± 0.66
Laser step 18	4.383	0.0129	0.090	0.00225	84.9	3.719	92.11	64.64 ± 0.66
Laser step 19	4.358	0.0124	0.088	0.00210	85.8	3.738	100.00	64.96 ± 0.69
Weighted mean								64.85 ± 0.74
Plateau								64.49 ± 0.22
50/652 (C)								
Step 1	9.653	0.0163	0.281	0.02067	36.7	3.546	4.24	61.69 ± 0.64
Step 2	4.615	0.0118	0.247	0.00268	82.8	3.822	5.90	66.41 ± 0.66
Step 3	4.524	0.0126	0.340	0.00210	86.3	3.904	12.24	67.80 ± 0.73
Step 4	4.253	0.0122	0.354	0.00137	90.5	3.848	18.21	66.84 ± 0.72
Step 5	4.085	0.0123	0.330	0.00110	92.1	3.762	27.36	65.37 ± 0.68
Step 6	4.084	0.0125	0.253	0.00118	91.5	3.735	34.61	64.92 ± 0.70
Step 7	4.100	0.0126	0.204	0.00124	91.1	3.733	46.17	64.88 ± 0.66
Step 8	4.126	0.0126	0.134	0.00140	90.0	3.713	57.14	64.54 ± 0.68
Step 9	4.188	0.0121	0.121	0.00153	89.2	3.736	65.78	64.94 ± 0.68
Step 10	4.250	0.0121	0.110	0.00165	88.5	3.763	72.37	65.39 ± 0.72
Step 11	4.228	0.0130	0.123	0.00170	88.2	3.727	82.80	64.78 ± 0.67
Step 12	4.241	0.0124	0.147	0.00182	87.4	3.705	96.21	64.40 ± 0.65
Step 13	4.328	0.0128	0.145	0.00206	85.9	3.719	100.00	64.63 ± 0.80
Weighted mean								65.21 ± 0.71
Plateau								64.87 ± 0.23
50/710	*J* value = 0.009787							
Step 1	8.056	0.0152	0.205	0.01387	49.1	3.958	4.4	68.56 ± 0.90
Step 2	4.348	0.0130	0.186	0.00192	86.9	3.779	6.8	65.52 ± 1.03
Step 3	4.246	0.0120	0.210	0.00152	89.4	3.796	14.2	65.80 ± 0.69
Step 4	4.059	0.0120	0.199	0.00093	93.2	3.783	20.3	65.60 ± 0.70
Step 5	4.005	0.0122	0.207	0.00074	94.5	3.787	24.4	65.65 ± 0.76
Step 6	3.956	0.0114	0.189	0.00066	95.1	3.837	31.3	65.23 ± 0.68
Step 7	3.937	0.0113	0.197	0.00062	95.3	3.828	39.0	65.08 ± 0.67
Step 8	3.919	0.0115	0.173	0.00052	96.1	3.879	45.9	65.29 ± 0.68
Step 9	3.942	0.0115	0.166	0.00059	95.6	3.842	51.0	65.31 ± 0.72
Step 10	4.020	0.0120	0.153	0.00083	93.9	3.773	59.1	65.42 ± 0.96
Step 11	4.072	0.0118	0.135	0.00099	92.8	3.779	65.9	65.51 ± 0.70
Step 12	4.114	0.0119	0.129	0.00126	90.9	3.741	71.9	64.88 ± 0.73
Step 13	4.150	0.0121	0.127	0.00127	90.9	3.774	77.9	65.44 ± 0.75
Step 14	4.193	0.0130	0.123	0.00160	88.7	3.719	80.8	64.50 ± 0.91
Step 15	4.258	0.0131	0.124	0.00185	87.2	3.712	83.1	64.38 ± 0.90
Step 16	4.297	0.0128	0.117	0.00197	86.5	3.715	85.8	64.43 ± 0.83
Step 17	4.336	0.0130	0.123	0.00172	88.3	3.829	89.5	66.37 ± 0.77
Step 18	4.336	0.0128	0.133	0.00178	87.9	3.811	91.8	66.06 ± 1.37
Step 19	4.427	0.0116	0.144	0.00246	83.6	3.701	94.0	64.19 ± 1.09
Step 20	4.354	0.0129	0.142	0.00225	84.7	3.688	96.0	63.97 ± 1.15
Step 21	4.321	0.0120	0.144	0.00183	87.5	3.779	100.0	65.53 ± 0.89
Weighted mean								65.40 ± 0.39
Plateau								65.38 ± 0.21

All analytical errors shown at 2σ with *J* value errors included.
*All final age errors at 95% confidence level.
†Errors on the *J* value determinations are 0.5%.

the first steps, and yielded a plateau with an age of 64.49 ± 0.22 Ma over 77.5% of the ^{39}Ar release (Fig. 3d). A third aliquot yielded a plateau age of 64.87 ± 0.23 Ma over 81.8% of ^{39}Ar release (Fig. 3d). All three samples yielded similar Ca/K ratio *vs.* ^{39}Ar release patterns, rising initially then falling to lower values but the two samples which yielded plateaus exhibited higher Ca/K values and reached a plateau after around 50–60% release. Also unlike the first aliquot, the later two yielded slightly high ages in the first few percent of ^{39}Ar release.

The sample at 622 m depth exhibited zoned feldspars with cores containing a mean of 0.48% K_2O, and rims with up to 11.76% K_2O. Analyses of clear glass yielded a mean of 0.028% K_2O, a small area of devitrified glass contained 0.22% K_2O and an area of altered glass and clay minerals contained 0.81% K_2O. A Z-contrast image (Fig. 2c) illustrates the morphology of the feldspar laths in this sample and a potassium x-ray map (Fig. 2d) shows just how strongly the feldspars are zoned. The potassium-rich zones reach up to 100 μm in length but are rarely wider than 20 μm. Both aliquots yielded similar age patterns, initially high ages in the first release (Table 2) were followed by a flat portion and low ages in the final 20% of ^{39}Ar release. In both cases the drop in ages was accompanied by a jump in Ca/K reflecting argon release from a new calcium-rich phase. None of the other samples exhibited low ages at the end of the release and it seems likely that the higher initial ages and lower late ages are the result of ^{39}Ar recoil during the irradiation. This effect is common in fine-grained igneous rocks and results when ^{39}Ar created from potassium in a potassium-rich mineral, most probably the alkali feldspar, is recoiled into a potassium-poor mineral which released argon at higher temperatures. It is unclear however why recoil was important in this sample when it was not observed in sample 50/652 which has a very similar mix of minerals and glass. One aliquot exhibited a long central portion of similar ages but variation was sufficient to prevent it reaching the criteria for a plateau. The second sample yielded a plateau age of 65.22 ± 0.24 Ma over 62.5% of the ^{39}Ar release (Fig. 3e).

The final sample taken at a depth of 605 m exhibits similar textures to sample 50/622. Two aliquots were analysed, both yielding very similar percent ^{39}Ar release patterns and Ca/K variations (Table 2). Initially high ages ~70 Ma fall to a flat portion around 67–68 Ma before becoming less stable and rising in the later release. Ca/K ratios show a very strong variation, falling from initial values ~0.45 to as low as 0.22 before rising steeply back to the original value. This is the only sample to exhibit such a strong rise, probably reflecting its higher feldspar clast content. Only one of the aliquots yielded a plateau age which was 67.84 ± 0.44 Ma over 60.7% of release (Fig. 3f), though this was a small sample and errors are higher than the other step-heated samples. The release spectrum exhibits a saddle shape, often considered indicative of excess argon, but an isochron of the plateau data yields an age of 67.2 ± 1.1 Ma with a $^{40}Ar/^{36}Ar$ intercept of 326 ± 111. On its own, this result could be interpreted as an age with the small scatter resulting from a mixture of radiogenic argon and modern atmospheric argon, or the data might also indicate a mixing line between a homogeneous excess argon and modern atmospheric argon (*e.g.*, Sherlock and Arnaud, 1999). Both interpretations are equally valid based on this sample alone.

Considering all the samples, three did not yield reproducible ages, four yielded plateau ages. A weighted mean of all the plateau ages is 65 ± 1 Ma (95% confidence level; Ludwig, 1999) when the errors are enhanced using the square root of the mean square of weighted deviates (which was 49 indicative of the large spread in comparison with analytical errors). Note that the ages obtained from glass samples of the Chixculub impact yielded ages of 65.46 ± 0.6 Ma when recalculated to the same standard as used in the present study (Renne *et al.*, 1998). We are probably justified in refining the age further by removing sample 50/605, since its age is significantly older than the others and it exhibited a saddle-shaped release spectrum. The mean age of the best analysis from each of the remaining three samples (50/622, 50/652 and 50/710) is 65.17 ± 0.64 Ma (95% confidence level). This age still falls within errors of the age for the samples of Chixculub (65.46 ± 0.6 Ma, recalculated by Renne *et al.*, 1998). Further refinement of the age is not justified on the basis of this data set.

Ar-Ar geochronology has indicated end-Cretaceous ages for other impacts, but several criteria give us confidence that this age for the Boltysh impact is robust. Firstly, the age reflects isotopic analyses of three different samples, and chemical analyses show that while the age reflects radiogenic argon in the glass in sample 50/710, samples 50/652 and 50/622 are dominated by radiogenic argon in alkali feldspars. Moreover the samples were irradiated and analysed often in duplicate, over a period of more than a year. Secondly, samples yielding older ages, tend to be those from glass-rich layers in the bore hole (Fig. 4), and show mineral textures which indicate rapid crystallization and quenching, which might be expected to preserve radiogenic argon from the target rock. Samples showing greater proportions of crystals tend to be those which yield younger and more reproducible ages. Finally, the new Ar-Ar age coincides closely with a recent fission track age of 65 ± 1 Ma (1σ errors) (Kashkarov *et al.*, 1998) from a sample at a similar depth in an adjacent borehole.

CRATERING RATES AND CRATER CLUSTERS

The fact that the isotopic ages of the Chixculub and Boltysh impacts are in distinguishable does not prove that they combined to lead to the mass extinction at the end of the Cretaceous period. Note that the Popagai impact (100 km diameter) and Chesapeake Bay impact (80 km) have indistinguishable isotopic ages but gave rise to separate microspherule horizons and did not cause a mass extinction.

If we were to apply statistics to the probability of coincidence between the isotopic ages for Boltysh and Chixculub impacts, we would obtain overwhelming evidence

for coincidence, but this reflects the errors on the isotopic dating and does not constitute proof that the two impacts were synchronous. The coincidence of the Chixculub event with the K/T boundary is now constrained to within a few thousand years (*e.g.*, Mukhopadhyay *et al.*, 2001; Norris *et al.*, 1999), using the stratigraphic record of ejecta in deep sea cores. However, it may be possible to test the synchronicity of Boltysh and Chixculub by careful study of K/T sites close to Boltysh which clearly produced a significant ejecta layer (Gurov *et al.*, 2001). Several anomalous aspects of the distal ejecta layers associated with the K/T boundary may be linked to an input from Boltysh, for example, reversed grading in the Petruccio section (Montanari, 1990), though this may also be explained by redistribution during sedimentary processes. Variations in the global distribution of Ni-rich spinels and differences in Cr content between European sites might indicate multiple impacts. Indeed Robin *et al.* (1993) suggested that variations in spinel compositions may be the result of atmospheric ablation of many bolides. However, the similarity in layer thickness and morphology at all K/T sites distal from Chixculub tends to indicate that the bulk of them were derived from one impact (Smit, 1999).

Terrestrial cratering rates have been estimated by several different methods. Shoemaker and Shoemaker (1996) estimated a cratering rate for the Proterozoic in Australia of $(3.8 \pm 1.9) \times 10^{-15}$ km^{-2}/year, and $(6.3 \pm 3.2) \times 10^{-15}$ km^{-2}/year (by extrapolation from impact structures larger than 10 km) for the Phanerozoic in the USA. Grieve and Shoemaker (1994) estimated the cratering rate since 120 Ma to be $(5.6 \pm 2.8) \times 10^{-15}$ km^{-2}/year, and Grieve and Pesonen (1996) estimated the cratering rate for craters larger than 20 km as $(5.5 \pm 2.7) \times 10^{-15}$ km^{-2}/year. Finally, Hughes (2000) calculated a more conservative cratering rate estimate of $(3.0 \pm 0.3) \times 10^{-15}$ km^{-2}/year for craters larger than 22 km, based upon a re-examination using the mean areas of craters, together with the gradients of linear plots of crater numbers *vs.* crater ages. Taking the most recent estimates of cratering rate (Grieve and Pesonen, 1996; Hughes, 2000) and the power law relationship between the cumulative number of craters N, and crater diameter D_c to be $N \propto D_c^{-1.8}$ (Shoemaker and Shoemaker, 1996), it is possible to show that there are "on average" 1.5 to 2.8 impacts capable of creating craters larger than 20 km on the Earth's surface every million years. Neglecting oceanic impacts, since both Chixculub and Boltysh impacts are on continental crust, reduces this to one impact every 1.8 to 3.3 Ma. Although these numbers can only be indicative, since cratering is an inherently random process, coincidence might explain one 20 km terrestrial impact crater forming within half a million years of the Chixculub impact. However, this is an unusual coincidence, in comparison with the known cratering record of the last 10 Ma. In fact, the most recent large impact of a similar size to Boltysh formed the Ries Crater in Germany 14.8 ± 0.1 Ma ago (Grieve, 1991). In other words there should be around eight undiscovered 20 km continental impact craters younger than the Ries Crater. Against this, the coincidence of two continental impacts within half a million years of the K/T boundary might seem unusual but it is not outside the bounds of "normal" cratering during the Paleozoic. If other craters should prove to have formed at the same time however, the paradigm of a single massive impact at the end-Cretaceous will have to be re-examined.

Acknowledgements–The authors acknowledge assistance from the Open University and Institute of Geological Sciences, National Academy of Ukraine. Sarah Sherlock kindly read an earlier version of this manuscript and helpful reviews were provided by Paul Layer and Mike Villeneuve.

Editorial handling: R. A. F. Grieve

REFERENCES

ALVAREZ L. W., ALVAREZ W., ASARO F. AND MICHEL H. V. (1980) Extraterrestrial cause for the Cretaceous–Tertiary extinction. *Science* **208**, 1095–1108.

BOIKO A. K., VALTER A. A. AND VISCHNYAK A. F. (1985) About the age of the Boltysh depression (in Russian). *Geologichesky Zhurnal* **45**, 86–90.

BOTTOMLEY R., GRIEVE R., YORK D. AND MASAITIS V. (1997) The age of the Popigai impact event and its relation to events at the Eocene/Oligocene boundary. *Nature* **388**, 365–368.

CLAEYS P. AND CASIER J. G. (1994) Microtektite-like impact glass associated with the Frasnian–Famennian boundary mass extinction. *Earth Planet. Sci. Lett.* **122**, 303–315.

FARLEY K. A., MONTANARI A., SHOEMAKER E. M. AND SHOEMAKER C. S. (1998) Geochemical evidence for a comet shower in the Late Eocene. *Science* **280**, 1250–1253.

GLASS B. P., HALL C. M. AND YORK D. (1986) ^{40}Ar-^{39}Ar laser-probe dating of North-American tektite fragments from Barbados and the age of the Eocene–Oligocene boundary. *Chem. Geol.* **59**, 181–186.

GRIEVE R. A. F. (1991) Terrestrial impact—The record in the rocks. *Meteoritics* **26**, 175–194.

GRIEVE R. A. F. AND PESONEN L. J. (1996) Terrestrial impact craters: Their spatial and temporal distribution and impacting bodies. *Earth Moon Planets* **72**, 357–376.

GRIEVE R. A. F. AND SHOEMAKER E. M. (1994) The record of past impacts on Earth. In *Hazards Due to Comets and Asteroids* (ed. T. Gehrels), pp. 417–462. Univ. Arizona Press, Tucson. Arizona, USA.

GRIEVE R. A. F., RENY G., GUROV E. P. AND RYABENKO V. A. (1987) The melt rocks of the Boltysh impact crater, Ukraine, USSR. *Contrib. Mineral. Petrol.* **96**, 56–62.

GUROV E. P. AND BABINA N. V. (2000) Formation of the Boltysh impact structure: Catastrophe of regional scale (abstract). In *Catastrophic Events and Mass Extinctions: Impacts and Beyond* (ed. C. Koeberl), pp. 62. Lunar and Planetary Institute Contribution **1053**, Houston, Texas, USA.

GUROV E. P. AND GUROVA E. P. (1991) *Geological Structure and Composition of Rocks in Impact Structures* (in Russian). Naukova Dumka Press, Kiev, Ukraine. 160 pp.

GUROV E., KELLEY S. P. AND KOEBERL C. (2002) Ejecta of the Boltysh impact crater in the Ukrainian Shield. In *Lecture Notes in Earth Sciences: Impact Studies* (eds. C. Koeberl and F. M. Ruiz). Springer, Berlin, Germany (in press).

HUGHES D. W. (2000) A new approach to the calculation of the cratering record of the Earth over the last 125 ± 20 Myr. *Monthly Notices Royal Astron. Soc.* **317**, 429–437.

IZETT G. A., COBBAN W. A., OBRADOVICH J. D. AND KUNK M. J. (1993) The Manson impact structure—Ar-40/Ar-39 age and its

distal impact ejecta in the Pierre shale in southeastern South-Dakota. *Science* **262**, 729–732.

KASHKAROV L. L., NAZAROV M. A., KALININA G. V., LORENZ K. A. AND KONONKOVA N. N. (1998) Fission track dating of the Boltysh impact crater, Ukraine (abstract). *Lunar Planet. Sci.* **29**, #1257, Lunar and Planetary Institute, Houston, Texas, USA (CD-ROM).

KOEBERL C., SHARPTON V. L., MURALI A. V. AND BURKE K. (1990) Kara and Ust-Kara impact structures (USSR) and their relevance to the K/T boundary event. *Geology* **18**, 50–53.

KOEBERL C., ARMSTRONG R. A. AND REIMOLD W. U. (1997) Morokweng, South Africa: A large impact structure of Jurassic–Cretaceous boundary age. *Geology* **25**, 731–734.

KOMAROV A. N. AND RAICHLIN A. I. (1976) Comparative study of impactite age by fission track and K-Ar methods (in Russian). *Doklady Academii Nauk USSR* **228**, 673–676.

KUNK M. J., IZETT G. A., HAUGERUD R. A. AND SUTTER J. F. (1989) Ar-40-Ar-39 dating of the Manson impact structure—A Cretaceous–Tertiary boundary crater candidate. *Science* **244**, 1565–1568.

LUDWIG K. R. (1999) *Isoplot/Ex 2.01: A Geochronological Toolkit for Microsoft Excel*. Berkeley Geochronology Center, Berkeley, California, USA. 50 pp.

MONTANARI A. (1990) Authigenesis of impact spheroids in the K/T boundary clay from Italy: New constraints for high-resolution stratigraphy of terminal cretaceous events. *J. Sediment. Petrol.* **61**, 315–339.

MUKHOPADHYAY S., FARLEY K. A. AND MONTANARI A. (2001) A short duration of the Cretaceous–Tertiary boundary event: Evidence from extraterrestrial helium-3. *Science* **291**, 1952–1955.

NORRIS R. D., HUBER B. T. AND SELF-TRAIL J. (1999) Synchroneity of the K–T oceanic mass extinction and meteorite impact: Blake Nose, western North Atlantic. *Geology* **27**, 419–422.

RAMPINO M. (1998) The galactic theory of mass extinctions: An update. *Celestial Mechanics Dynamical Astronomy* **69**, 49–58.

RENNE P. R., SWISHER C. C., DEINO A. L., KARNER D. B., OWENS T. L. AND DEPAOLO D. J. (1998) Intercalibation of standards, absolute ages and uncertainties in $^{40}Ar/^{39}Ar$ dating. *Chem. Geol.* **145**, 117–152.

ROBIN E., FROGET L., JEHANNO C. AND ROCCHIA R. (1993) Evidence for a K/T impact in the Pacific Ocean. *Nature* **363**, 615–618.

SHERLOCK S. C. AND ARNAUD N. O. (1999) Flat plateau and impossible isochrons: Apparent ^{40}Ar-^{39}Ar geochronology in a high-pressure terrain. *Geochim. Cosmochim. Acta* **63**, 2835–2838.

SHOEMAKER E. M. AND SHOEMAKER C. S. (1996) The Proterozoic impact record of Australia. *AGSO J. Australian Geol. Geophys.* **16**, 379–398.

SHUKULOKOV Y. A., KOLESNIKOV E. M., NAZAROV M. A., BADJOKOV D. D. AND KORINA M. I. (1988) K-Ar age of Kara impact structure—Evidence for its link with Cretaceous–Tertiary (K/T) event. *Chem. Geol.* **70**, 121–121.

SMIT J. (1999) The global stratigraphy of the Cretaceous–Tertiary boundary impact ejecta. *Ann. Rev. Earth Planet. Sci.* **27**, 75–113.

SPRAY J. G., KELLEY S. P. AND ROWLEY D. B. (1998) Evidence for a late Triassic multiple impact event on Earth. *Nature* **392**, 171–173.

STANISLAVSKY F. A. (1968) Age and stratigraphy of the sapropelites of the Boltysh depression (in Russian). *Geologichny Zhurnal* **28**, 105–110.

TRIELOFF M., DEUTSCH A. AND JESSBERGER E. K. (1998) The age of the Kara impact structure, Russia. *Meteorit. Planet. Sci.* **32**, 361–372.

ZEITLER P. K. (1996) $^{40}Ar/^{39}Ar$ thermochronology of shocked feldspars from the Manson impact structure. In *The Manson Impact Structure* (eds. C. Koeberl and R. R. Anderson), pp. 383–396. Geological Society of America, Boulder, Colorado, USA.